Stripe order and quasiparticle Nernst effect in cuprate superconductors

2010 New J. Phys. 12 105011

(http://iopscience.iop.org/1367-2630/12/10/105011)

New Journal of Physics
The open-access journal for physics

Stripe order and quasiparticle Nernst effect in cuprate superconductors

Andreas Hackl[1,3] **and Matthias Vojta**[2]

[1] Department of Physics, California Institute of Technology, Pasadena, CA 91125, USA

[2] Institut für Theoretische Physik, Technische Universität Dresden, 01062 Dresden, Germany

E-mail: ahackl@caltech.edu

New Journal of Physics **12** (2010) 105011 (17pp)
Received 31 July 2010
Published 29 October 2010
Online at http://www.njp.org/
doi:10.1088/1367-2630/12/10/105011

Abstract. After a brief review of current ideas on stripe order in cuprate high-temperature superconductors, we discuss the quasiparticle Nernst effect in cuprates, with focus on its evolution in non-superconducting stripe and related nematic states. In general, we find the Nernst signal to be strongly enhanced by nearby van-Hove singularities and Lifshitz transitions in the band structure, implying that phases with translation symmetry breaking often lead to a large quasiparticle Nernst effect due to the presence of multiple small Fermi pockets. Open orbits may contribute to the Nernst signal as well, but in a strongly anisotropic fashion. We discuss our results in the light of recent proposals for a specific Lifshitz transition in underdoped $YBa_2Cu_3O_y$ and make predictions for the doping dependence of the Nernst signal.

[3] Author to whom any correspondence should be addressed.

Contents

1. Introduction

Cuprate high-temperature superconductors continue to hold unsolved puzzles, one of them being the origin of the so-called pseudogap regime [1]. Various explanations have been proposed for this apparent suppression of spectral weight, which occurs below the doping-dependent pseudogap temperature T^*. These proposals include phase-incoherent Cooper pairing, symmetry-breaking orders competing with superconductivity, exotic fractionalized states and short-range singlet correlations as a precursor to the half-filled Mott insulator [2, 3].

Stripe order [4]–[7] takes a prominent role in cuprate phenomenology: such periodic modulations of spin and charge densities have been established to exist in the $La_{2-x}Sr_xCuO_4$ (or 214) family of cuprates, using a variety of experimental techniques, most importantly neutron and x-ray scattering [8]. Signatures of stripes also appear in experiments on other cuprate families, albeit providing less conclusive evidence, either because the experimental probes are restricted to the sample surface (e.g. scanning tunneling microscopy (STM) [9]–[11]) or because stripe physics is only probed indirectly (e.g. via finite-energy spin fluctuations, phonon anomalies or quantum oscillations) [7]. Collectively, the observations suggest that the tendency toward stripe order is a common phenomenon in underdoped cuprates. Then, while in some cuprates the stripe order is strong and static, in others it is presumably fluctuating in space and time, with the possibility of being pinned by impurities [5]–[7].

An interesting probe of pseudogap physics is provided by the transverse thermoelectric response, also known as the Nernst effect. While typically small in conventional metals, large positive Nernst signals are known to arise from the motion of vortices in type-II

superconductors [12, 13]. In addition, it has been pointed out that a large Nernst signal (of either sign) can occur in metals with a small (effective) Fermi energy [14]. Nernst measurements in cuprates, showing a rise of the Nernst signal at temperatures above the superconducting T_c, have been commonly interpreted as evidence for fluctuating Cooper pairs above T_c [15, 16]. However, this Nernst onset temperature appears to lie below the pseudogap temperature T^* identified by other probes, indicating that fluctuating Cooper pairs do *not* account for all of the cuprate pseudogap.

Recent Nernst measurements on underdoped cuprates have revealed additional information: in stripe-ordered $La_{1.6-x}Nd_{0.4}Sr_xCuO_4$ the temperature dependence of the Nernst signal shows an additional (positive) peak or shoulder at intermediate temperatures, which was tentatively attributed to a Fermi-surface reconstruction due to density-wave order [17]. (Note that this interpretation has been questioned by others [18]). In de-twinned crystals of $YBa_2Cu_3O_y$ (YBCO), the normal-state Nernst signal was found to be negative [19] and to display a huge temperature-dependent in-plane anisotropy [20]. The latter fact appears to tie in with the tendency to electron-nematic order, previously identified in neutron-scattering measurements on YBCO-6.45 [21].

These measurements underline the importance of understanding the quasiparticle Nernst effect in cuprates. Theoretically, the Nernst response has been calculated in simple quasiparticle models, and it has been shown that density-wave order can indeed lead to an enhanced Nernst signal [22]–[26], with the sign depending on the spatial periodicity and other details of the ordering pattern [25]. Further, Fermi-surface distortions as expected for electron-nematic order in the d-wave channel have been shown to induce huge Nernst anisotropies [27], in semi-quantitative agreement with the experimental data [20]. These results suggest (together with successful descriptions of transport and quantum oscillation data using related models [28]–[32]) that scenarios of Fermi-liquid-like quasiparticles, moving in states with lattice symmetry breaking, capture some important properties of underdoped cuprates.

The purpose of this paper is twofold. Firstly, we briefly review current ideas on the origin of stripe order in cuprates, together with its effect on the fermionic quasiparticle spectrum. Nematic order as a precursor of uni-directional stripes will naturally appear in the discussion. Secondly, we summarize and extend theoretical results for the quasiparticle Nernst effect in the normal state of stripe-ordered cuprates [25], also discussing the anisotropy of the Nernst signal. In particular, we focus on the Lifshitz transition where electron pockets near $(\pi, 0)$ disappear as doping is reduced, as recently proposed [32] for underdoped $YBa_2Cu_3O_y$ on the basis of quantum oscillation experiments [33]. While small Fermi pockets induce a strongly enhanced Nernst signal in both directions, open orbits appreciably contribute to the Nernst response only for a temperature gradient applied parallel to the dominant hopping direction. This allows specific predictions for the normal-state Nernst signal across the Lifshitz transition.

1.1. Outline

The body of this paper is organized as follows: In section 2, we start with an overview on selected aspects of stripe physics that we consider relevant for the Nernst effect and its evolution within the cuprate phase diagram. Section 3 contains a brief general discussion of thermoelectric effects with focus on the quasiparticle Nernst signal. Section 4 then describes the concrete model and calculational scheme that we employ to investigate the quasiparticle Nernst effect in the normal state of cuprates. The results from this approach are discussed in section 5, where we

both review selected earlier results of [25, 27] and present new ones that are relevant for the strongly underdoped regime. A discussion of experimental implications and an outlook close the paper.

2. Stripe order in cuprates

Density-wave order in cuprates has been the subject of numerous review articles in the past [4]–[7], but new experiments continue to shape (and sometimes change) our view on this fascinating set of phenomena. We shall use this section to give a brief overview, combining experimental and theoretical aspects, regarding two central aspects, namely the cause of stripe formation and the nature of fermionic single-particle excitations in stripe phases.

2.1. Order parameters and symmetry breaking

To set the stage, we repeat the standard definitions of order parameters that are relevant for unidirectional stripe order in quasi-2D systems such as cuprates. In all cases, we employ a language appropriate for slowly varying order parameter fields.

First, a charge density wave (CDW) is described by a pair of complex scalar fields ϕ_{cx}, ϕ_{cy} for the two CDW directions with wavevectors $\vec{Q}_{cx}$ and $\vec{Q}_{cy}$. The charge density is assumed to obey

$$\langle \rho(\vec{R}, \tau) \rangle = \rho_{\text{avg}} + Re[e^{i\vec{Q}_c \cdot \vec{R}} \phi_c(\vec{R}, \tau)]. \tag{1}$$

The spin density wave (SDW) is assumed to be collinear [34][4]. Then, a pair of complex vector fields $\phi_{s\alpha x}$, $\phi_{s\alpha y}$, $\alpha = x, y, z$, captures SDW correlations with wavevectors $\vec{Q}_{sx}$ and $\vec{Q}_{sy}$, with the spin density following

$$\langle S_\alpha(\vec{R}, \tau) \rangle = Re\left[e^{i\vec{Q}_s \cdot \vec{R}} \phi_{s\alpha}(\vec{R}, \tau)\right]. \tag{2}$$

Experimentally, order has been found at $\vec{Q}_{sx} = 2\pi(0.5 \pm 1/M, 0.5)$, $\vec{Q}_{sy} = 2\pi(0.5, 0.5 \pm 1/M)$ and $\vec{Q}_{cx} = (2\pi/N, 0)$, $\vec{Q}_{cy} = (0, 2\pi/N)$, where M and N are the real-space periodicities that follow $M = 2N$ to a good accuracy [5]–[8].

As argued in [35], introducing a separate order parameter for rotational symmetry breaking in a tetragonal environment is useful: this is an Ising scalar ϕ_n for $l = 2$ spin-symmetric electron-nematic order, which carries wavevector $\vec{Q} = 0$. It is common practice to refer to ϕ_n as nematic order parameter. Care is required in the terminology: strictly speaking, a nematic phase is one with $\phi_n \neq 0$ and $\phi_c = \phi_s = 0$; phases with e.g. $\phi_c \neq 0$ have $\phi_n \neq 0$ as well, but are not to be called nematic (but smectic).

In a number of cuprates, the tetragonal in-plane symmetry is broken down to orthorhombic, and spontaneous nematic order cannot exist. It may still make sense to discuss the tendency toward electron-nematic order if the microscopic anisotropy is strongly enhanced by electronic correlation effects.

[4] Although spin-spiral order has been discussed for cuprates in the doping range above 5.5%, the simultaneous presence of spin and charge order in some 214 cuprates points toward collinear instead of spiral spin correlations in cuprates above 5.5% doping. Neutron scattering experiments are consistent with this view, but have not fully ruled out non-collinear states.

2.2. *Origin of stripes*

The driving force for stripe formation has been intensively discussed since stripes were discovered. Conceptually, weak-coupling and strong-coupling approaches need to be distinguished.

On the one hand, weak coupling refers to density-wave instabilities that can be obtained in perturbation theory with a Fermi-liquid picture. In the simplest case, random-phase approximation (RPA) is used for a given dispersion of single-particle excitations to obtain the ordering wavevector from the pole in static susceptibility. This concept relies on the existence of well-defined quasiparticles with significant weight and ties the ordering to properties of the Fermi surface.

On the other hand, strong-coupling ideas come in various flavors, and most often they do not relate to properties of the single-particle sector. Popular lines of thought are (A) frustrated phase separation, (B) spin-charge 'topological' properties and (C) valence-bond solid formation, all of which have been invoked to rationalize the formation of conducting stripes in cuprates. While (A) is general, (B) and (C) refer to more microscopic aspects.

The idea of frustrated phase separation [36]–[38] builds on the assumption that, without long-range Coulomb repulsion, a doped Mott insulator is unstable toward phase separation, i.e. the Mott insulator tends to expel holes. Then, including Coulomb repulsion leads to domain formation; in the simplest case these domains are linear. (More generally, particles on a lattice, moving under the influence of short-range attractions and long-range repulsions, minimize their energy by forming domains with modulated density.) It must be noted, however, that the existence of phase separation in the Hubbard or t–J models in the relevant regime of parameters is questionable, considering a body of numerical results where phase separation is only seen in the t–J model at large J/t and small doping.

The co-existence of spin and charge order, with hole-rich stripes being anti-phase domain walls of the underlying antiferromagnetism, has led to interpretations of stripes as a 2D generalization of holons [39]. This concept suggests that magnetic order is a prerequisite for stripe formation; however, at least some compounds ($La_{2-x}Ba_xCuO_4$, Eu and Nd co-doped $La_{2-x}Sr_xCuO_4$) display a temperature range with long-range charge order but without long-range magnetic order [7].

Finally, the valence-bond solid idea is based on the tendency of paramagnetic Mott insulators on the square lattice to break translation and rotation symmetry in the form of a columnar valence-bond solid [40]. Upon doping, stripes are assumed to inherit this type of symmetry breaking, with an additional modulation in the hole density [41].

To date, the question about the origin of stripes is not settled. Many cuprate experiments point toward a strong-coupling picture as being more appropriate than a weak-coupling one [5]–[7]. One central argument here is about the evolution of the charge-ordering wavevector with doping x in 214 compounds, $\vec{Q}_c \approx (4\pi x, 0)$ for $x < 1/8$, which is opposite to the evolution of possible Fermi-surface nesting wavevectors; others are about the intensity of the magnetic response (too large to be compatible with RPA) and the pinning of stripes by impurity doping (which is not expected in weak coupling). Which of the strong-coupling ideas is closest to reality is not obvious. Recent STM experiments [11], showing bond-centered stripes with strong bond modulations on the surface of two different cuprates, lend some support to the valence-bond solid idea, although a detailed understanding of the role of oxygen orbitals is lacking.

2.3. Fermionic quasiparticles in stripe phases

Low-temperature dc transport is generically determined by the properties of the low-energy charge carriers. Various low-temperature experiments, most notably those involving quantum oscillations, indicate that charge carriers in underdoped cuprates are Fermi-liquid-like quasiparticles [42, 43]. However, the temperature evolution of both thermodynamic and spectral properties does not easily fit into a conventional Fermi-liquid picture [1]. A generally accepted solution of this puzzle is not known to date.

The available proposals can be grouped into two classes:

(i) The low-doping state is asymptotically a conventional Fermi liquid (in the absence of superconductivity), but with both coherence temperature and quasiparticle weight being small. This implies e.g. that the Fermi surface of this state is 'large' (in the absence of translational symmetry breaking), i.e. it fulfills Luttinger's theorem. This large Fermi surface may be unobservable if translational symmetry breaking sets in above the coherence temperature.

(ii) The low-doping state is a metallic non-Fermi liquid. It may still feature Fermi-liquid-like quasiparticles, but Luttinger's theorem is violated. (A state of this type is the so-called fractionalized Fermi liquid, introduced for two-band models of heavy-fermion metals [44]). Theories of type (ii) find support in computational studies of the one-band Hubbard model using cluster extensions of dynamical mean-field theory [45]–[48]. These studies indicate that the low-doping metallic state is characterized by small Fermi pockets (in the absence of symmetry breaking), and transition to a conventional metal with a large Fermi surface occurs around optimal doping. A phenomenological ansatz for the self-energy describing a pseudogap state with small pockets has been put forward in [49].

In both scenarios, density-wave order will lead to a backfolding of the quasiparticle bands due to translational symmetry breaking. This invariably causes the existence of multiple Fermi pockets and/or open orbits, depending on the strength of density-wave order and other microscopic details.

To date, photoemission experiments have not been able to distinguish the available scenarios, mainly because of insufficient energy and momentum resolution (although progress has been made recently [50]). On the theory side, many papers start from the more conventional scenario (i) (often even approximating the quasiparticle weight by unity), which then allows one to perform concrete calculations of more complicated observables with moderate effort. Our calculations below will follow this route as well.

3. Nernst effect

The Nernst effect is the generation of a transverse electric field by a longitudinal thermal gradient in the presence of a finite magnetic field. Although the Nernst effect in cuprate superconductors has attracted some attention over the past years, the Nernst effect in correlated-electron metals in general is largely unexplored [14].

In linear-response theory, the thermoelectric response is captured by three conductivity tensors $\hat{\sigma}$, $\hat{\alpha}$ and $\hat{\kappa}$, which relate charge current $\vec{J}$ and heat current $\vec{Q}$ to electric field $\vec{E}$ and thermal gradient $\vec{\nabla}T$:

$$\begin{pmatrix} \vec{J} \\ \vec{Q} \end{pmatrix} = \begin{pmatrix} \hat{\sigma} & \hat{\alpha} \\ T\hat{\alpha} & \hat{\kappa} \end{pmatrix} \begin{pmatrix} \vec{E} \\ -\vec{\nabla}T \end{pmatrix}. \tag{3}$$

The electrical field induced by a thermal gradient in the absence of an electrical current can be expressed by the linear-response relation $\vec{E} = -\hat{\vartheta}\vec{\nabla}T$, and equation (3) together with $\vec{J} = 0$ yields $\vec{E} = \hat{\sigma}^{-1}\hat{\alpha}\vec{\nabla}T$. Therefore, the Nernst signal ϑ_{yx}, defined as the *transverse* voltage E_y generated by a thermal gradient $\nabla_x T$, reads

$$\vartheta_{yx} = -\frac{\sigma_{xx}\alpha_{yx} - \sigma_{yx}\alpha_{xx}}{\sigma_{xx}\sigma_{yy} - \sigma_{xy}\sigma_{yx}} \tag{4}$$

and ϑ_{xy} is obtained from $x \leftrightarrow y$. For a magnetic field $\vec{B} = B\hat{z}$ in the z-direction, the Nernst *coefficient* is usually defined as $\nu_{yx} = \vartheta_{yx}/B$, which tends to become field-independent at small B. We employ a sign convention such that the vortex Nernst coefficient is always positive (formally $\nu_{xy} = -\vartheta_{xy}/B$.[5] In general, the Nernst coefficient can be negative or positive, for example if it is caused by the flow of charged quasiparticles.

The quasiparticle Nernst effect in metals is often small, which can be rationalized by the so-called Sondheimer cancellation [51]: for a single parabolic band, the two contributions to ϑ (4) exactly balance each other. Generally, in any realistic system, such a cancellation will be incomplete. In systems with a small (effective) Fermi energy, the resulting Nernst signal can be large [14]. This consideration is likely of relevance for states with translational symmetry breaking where band backfolding produces small Fermi pockets, although equation (4) shows that, in the presence of multiple quasiparticle bands, the Nernst signal is not simply a superposition of the signals from the individual bands (even if this applies to the elements of the $\hat{\sigma}$ and $\hat{\alpha}$ tensors). Together, this makes it clear that the magnitude and sign of the quasiparticle Nernst signal in general depend on various microscopic details.

In systems with broken tetragonal symmetry, it is worth discussing the anisotropy of the Nernst signal, i.e. the difference between ϑ_{yx} and ϑ_{xy}, equation (4). Assuming Onsager reciprocity, the Hall conductivities obey $\sigma_{xy} = -\sigma_{yx}$ independent of the crystal symmetry. Such a relation does not hold for $\alpha_{xy,yx}$ in general; however, in the low-T limit the Mott relation can be derived from Boltzmann theory,

$$\alpha_{ij} = -\frac{\pi^2}{3}\frac{k_B^2 T}{e}\frac{\partial \sigma_{ij}}{\partial \mu}|_{E_F}, \tag{5}$$

implying that $\alpha_{xy} = -\alpha_{yx}$. Then, anisotropies in the Nernst signal can only arise from diagonal conductivity anisotropies, $\sigma_{xx} - \sigma_{yy} \neq 0$ and $\alpha_{xx} - \alpha_{yy} \neq 0$.

Strictly, Onsager reciprocity can only be proven if time-reversal symmetry is not spontaneously broken by the system. It has recently been proposed that a particular type of time-reversal symmetry breaking is at play in underdoped cuprates, leading to off-diagonal conductivity anisotropies [52]. Here, we shall restrict our attention to stripe (and related) states. Although magnetically ordered stripe states do break time reversal as well, such states do not lead to off-diagonal anisotropies within the Boltzmann framework described below in section 4.2, i.e. the above statements based on Onsager reciprocity do apply.

[5] For fixed magnetic field $\vec{B}||\hat{z}$, a C_4-symmetric situation yields $\vartheta_{xy} = -\vartheta_{yx}$ from equations (3) and (4). Here, we use the convention that the three vectors $\vec{E}$, $\vec{\nabla}T$ and $\vec{B}$ form a right-handed system for measurements of both ν_{xy} and ν_{yx}. Then, $\nu_{xy} = \nu_{yx}$ for C_4 symmetry.

4. Quasiparticle model and Boltzmann transport

To calculate the normal-state quasiparticle Nernst effect, we consider electrons moving on a square lattice of unit lattice constant, with the 2D dispersion given by

$$\varepsilon_k = -2t_1(\cos k_x + \cos k_y) - 4t_2 \cos k_x \cos k_y - 2t_3(\cos 2k_x + \cos 2k_y). \tag{6}$$

The hopping parameters are chosen as $t_1 = 0.38\,\mathrm{eV}$, $t_2 = -0.32t_1$ and $t_3 = -0.5t_2$ [53, 54], unless otherwise noted. The 2D electron density is $n = 1 - x$ per unit cell.

4.1. Mean-field theory for ordered states

As is standard and is described in much detail in [25, 27, 28, 30], we shall employ simple (non-self-consistent) mean-field approximations to capture the symmetry-broken states.

Electron-nematic order is captured by different hopping energies along the x- and y-axes. Hence, $t_{1x,y} = (1 \pm \epsilon/2)t_1$ and $t_{3x,y} = (1 \pm \epsilon/2)t_3$.

For stripes, quasiparticles with the dispersion (6) are subject to a periodic modulation in the site chemical potential or bond kinetic energy. The relevant modulations are described by

$$\hat{V}_1 = \sum_{\vec{k},\sigma} (V_\mathrm{c}(\vec{k}) c^\dagger_{\vec{k}+\vec{Q}_\mathrm{c}\sigma} c_{\vec{k}\sigma} + \mathrm{h.c.}) \tag{7}$$

for a CDW and by

$$\hat{V}_2 = \sum_{\vec{k},\sigma} \sigma\,(V_\mathrm{s}(\vec{k}) c^\dagger_{\vec{k}+\vec{Q}_\mathrm{s}\sigma} c_{\vec{k}\sigma} + \mathrm{h.c.}) \tag{8}$$

for a collinear SDW with polarization in the z-direction. In general, both $V_\mathrm{c}(\vec{k})$ and $V_\mathrm{s}(\vec{k})$ are complex, with the phase corresponding to a sliding degree of freedom. A site-centered CDW has modulated on-site chemical potentials, and we choose a real $V_\mathrm{c}(\vec{k}) \equiv -V_\mathrm{c}$. A bond-centered CDW with on-site modulations is characterized by $V_\mathrm{c}(\vec{k}) \equiv -V_\mathrm{c} e^{-iQ_\mathrm{c}/2}$; for modulations in the kinetic energy [41, 55] with primarily d-wave form factor, we have $V_\mathrm{c}(\vec{k}) = -\delta t\,(\cos(k_x + \frac{Q_\mathrm{c}}{2}) - \cos k_y) e^{-iQ_\mathrm{c}/2}$; in both cases $\vec{Q}_\mathrm{c} = (Q_\mathrm{c}, 0)$. A site-centered SDW has again a real $V_\mathrm{s}(\vec{k}) \equiv V_\mathrm{s}$, whereas a bond-centered SDW is captured by $V_\mathrm{s}(\vec{k}) \equiv -V_\mathrm{s}(1 + e^{-iQ_\mathrm{c}/2})/(2\cos(Q_\mathrm{c}/4))$ where $\vec{Q}_\mathrm{s} = (\pi \pm Q_\mathrm{c}/2, \pi)$. The complex phases of the CDW and SDW mean fields have been chosen such that the resulting order parameters ϕ_c and ϕ_s^2 are in-phase. Moreover, with positive V_c (site-centered) and positive δt (bond-centered) the resulting modulations are such that the electron density is small where the magnitude of the magnetic moment is small (i.e. near the anti-phase domain walls).

Various forms of $V_\mathrm{c}(\vec{k})$ and $V_\mathrm{s}(\vec{k})$ were used in [25]; below we will show the results for site-centered SDW modulations. Note that, on symmetry grounds, a mean-field Hamiltonian with a collinear SDW modulation only will induce a (parasitic) CDW with $\vec{Q}_\mathrm{c} = 2\vec{Q}_\mathrm{s}$.

4.2. Semiclassical transport

In the following, we shall calculate the low-temperature dc transport properties using a Boltzmann equation. We further assume, as is appropriate for low temperatures, that the relaxation is mainly due to randomly distributed impurities with a low density, leading to a

constant relaxation time $\tau_{\vec{k}} \equiv \tau_0$. To lowest order in the applied fields, the conductivities required to calculate the Nernst signal are given by

$$\begin{aligned}
\alpha_{xx} &= \frac{2e}{T} \sum_{\vec{k},n} \frac{\partial f^0_{\vec{k}}}{\partial \varepsilon_n(\vec{k})} \varepsilon_n(\vec{k}) \tau_0 (v^x_{\vec{k}})^2, \\
\alpha_{xy} &= \frac{2e^2 B}{T\hbar c} \sum_{\vec{k},n} \frac{\partial f^0_{\vec{k}}}{\partial \varepsilon_n(\vec{k})} \varepsilon_n(\vec{k}) \tau_0^2 v^x_{\vec{k}} \left[v^y_{\vec{k}} \frac{\partial v^y_{\vec{k}}}{\partial k_x} - v^x_{\vec{k}} \frac{\partial v^y_{\vec{k}}}{\partial k_y} \right], \\
\sigma_{xx} &= -2e^2 \sum_{\vec{k},n} \frac{\partial f^0_{\vec{k}}}{\partial \varepsilon_n(\vec{k})} \tau_0 (v^x_{\vec{k}})^2, \\
\sigma_{xy} &= -2\frac{e^3 B}{\hbar c} \sum_{\vec{k},n} \frac{\partial f^0_{\vec{k}}}{\partial \varepsilon_n(\vec{k})} \tau_0^2 v^x_{\vec{k}} \left[v^y_{\vec{k}} \frac{\partial v^y_{\vec{k}}}{\partial k_x} - v^x_{\vec{k}} \frac{\partial v^y_{\vec{k}}}{\partial k_y} \right],
\end{aligned} \tag{9}$$

where $\sum_n$ runs over the quasiparticle bands of the system in the presence of symmetry-breaking order, and $\varepsilon(\vec{k})$, $v_{\vec{k}}$ are the corresponding quasiparticle energies and velocities. We note that, in general, the current operators have inter-band contributions. However, those do not show up in the semiclassical Boltzmann equation, as the spectral functions appearing in the more general quantum Boltzmann equation are replaced by δ functions at the quasiparticle energies in the semiclassical limit. This approximation is justified for dc transport, provided that coherent quasiparticles exist. As a result, equations (9) are diagonal in the band index. A detailed derivation of equations (9) can be found e.g. in [25].

Within the Boltzmann framework and in the low-temperature limit, the Nernst coefficient ν is proportional to both the temperature T and the relaxation time τ_0.

5. Quasiparticle Nernst effect: results

In the remainder of the paper, we discuss the effect of the Fermi-surface reconstruction due to symmetry breaking on the normal-state Nernst effect in cuprates. Our focus will be on the underdoped regime. Here, both nematic and stripe order have found experimental support. While stripes have been established to exist in cuprates of the 214 family [7], the situation in YBCO is more involved: both neutron scattering [21] and transport [20] experiments have been interpreted in terms of electron-nematic order, setting in somewhere below the pseudogap line T^*, with static stripe order being absent in this regime. On the other hand, theoretical descriptions of Hall and quantum oscillation data using SDW mean-field pictures have been found to match experiments relatively well [28], [30]–[32] suggesting that SDW (or stripe) order is at least present in large magnetic fields of 15 T and above. Such field-induced order has been detected in neutron scattering in both 214 and YBCO cuprates [7, 56, 57]. Theoretically, the main driving mechanism is anticipated to be the competition between superconductivity and density-wave order [58].

5.1. Stripes and Lifshitz transitions

As pointed out above, the Fermi-surface reconstruction into pockets and open orbits will crucially influence the Nernst signal. A particularly interesting situation was advertised in [32]

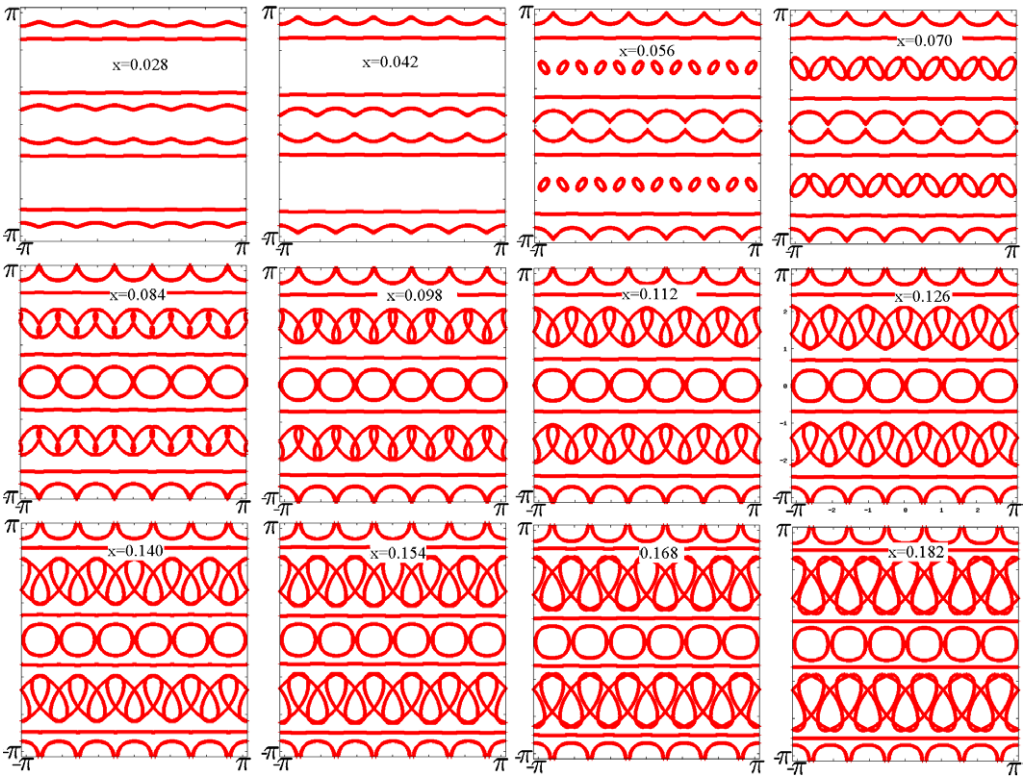

Figure 1. Fermi surfaces for vertical stripes with real-space period $M = 12$ for different doping values x. The bare quasiparticles, equation (6), are subject to a site-centered modulation in the spin sector, equation (8), with a doping-dependent strength $V_s(x) = (0.328 - x)$ eV ([32]). Various Lifshitz transitions are visible; in particular, the electron pockets near $(\pi, 0)$ merge into open orbits for $x \lesssim 8.5\%$.

for YBCO: it was argued that the electron pockets near $(\pi, 0)$, which have been made responsible for both the negative Hall effect [59] and the dominant quantum oscillations with 530 T oscillation frequency [60]–[62], disappear with decreasing doping, as a result of a strong stripe modulation in combination with a large spatial modulation period. The Lifshitz transition from a state with $(\pi, 0)$ pockets to a state without $(\pi, 0)$ pockets was proposed to be the origin of the divergence of the cyclotron mass upon lowering doping, as is observed in quantum oscillation measurements [33].

Figure 1 shows a sequence of Fermi surface plots for a (vertically striped) SDW state with real-space period $M = 12$ (implying a CDW period of $N = 6$) and varying doping. Thereby, it is assumed that the modulation strength follows $V_s(x) = (0.328 - x)$ eV. Note that, from experiments on 214 compounds [5]–[8], [63], $M = 12$ is known to be appropriate for doping $x \approx 1/12$; in [32] $M = 12$ was in fact employed, together with the above parametrization $V_s(x)$, to match quantum oscillation data over the entire doping range between 9 and 15%. (Clearly, $M = 12$ and $V_s(x)$ cease to be relevant to cuprates outside this doping window.) A more detailed modeling requires one to take into account the doping dependence of M (which moreover may depend on the applied field B as well). Unfortunately, $M(x, B)$ is not well known for

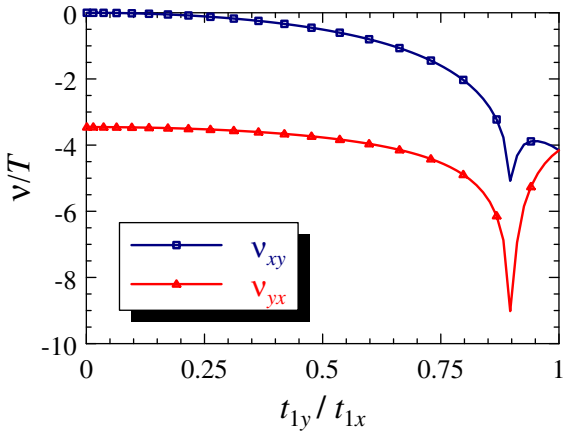

Figure 2. Nernst effect for a single band on a square lattice with anisotropic hopping. For $t_{1y}/t_{1x} < 0.9$, the Fermi surface consists of open orbits running along the $\hat{y}$ direction. For small t_{1y}, the Nernst signal develops a huge anisotropy. The units of ν/T are $10^5\ \mathrm{V/(K^2\,T)} \times \tau_0/\mathrm{s}$; here $t_{1x} = 1\,\mathrm{eV}$.

YBCO; therefore, we restrict our attention to $M = 12$, which we believe reproduces important qualitative aspects.

Technically, $M = 12$ implies the diagonalization of a 12×12 Hamiltonian matrix, in analogy to [25, 30]. We consider a site-centered spin-only modulation with $V_s(\vec{k}) = V_s$, unless otherwise noted.

The Fermi surfaces in figure 1 make it clear that a series of Lifshitz transitions can be expected as doping is varied. At dopings $x \geqslant 8.5\%$, various types of Fermi pockets are present; in particular, there are prominent electron pockets near $(0, \pi)$ and equivalent wavevectors. Those large electron pockets merge and disappear for $x \lesssim 8.5\%$, leaving only tiny electron pockets and open orbits. At around 7.5%, these tiny electron pockets transform into hole pockets, until, finally, for $x \lesssim 5\%$ all pockets disappear, and the resulting state displays exclusively open orbits. The presence of $(\pi, 0)$ electron pockets at dopings of 10% and higher is a robust feature of spin stripe order; see e.g. figure 2 of [32] and figures 2 and 3 of [25] for Fermi-surface results for $M = 8$ stripes[6]. In contrast, additional strong charge modulation may eliminate the electron pockets, figure 4(b) of [25].

5.2. *Nernst effect from open orbits*

Before discussing the Nernst effect over the entire doping range, we find it appropriate to separately analyze the Nernst signal arising from open Fermi orbits. Clearly, those will dominate in stripe-ordered cuprates at small doping, but the information here is also interesting on general grounds.

To illustrate the physics, we consider a simple tight-binding model on a square lattice, with nearest-neighbor hopping in the $\hat{x}$ direction, t_{1x} normalized to unity. We fix the hole doping at $x = 0.1$ and vary the nearest-neighbor hopping in the $\hat{y}$ direction, t_{1y}. Both Nernst signals, ν_{yx}/T and ν_{xy}/T, are displayed in figure 2 as a function of t_{1y}/t_{1x}. A van-Hove singularity

[6] In [25], the identification of pockets as electron-like or hole-like was partially incorrect. This concerns the captions of figures 2(b), 3 and 14. All numerical results of [25] remain unaffected.

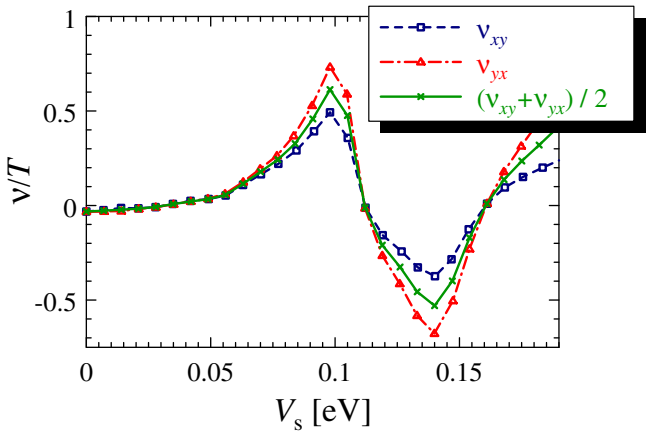

Figure 3. Nernst effect for period-8 antiferromagnetic stripes at doping $x = 1/8$ as a function of spin modulation. The bare quasiparticle dispersion is in equation (6). The Nernst coefficient becomes negative at $V_s \simeq 0.1\,\text{eV}$, corresponding to maximal local moments of $2\mu_B\langle S_z\rangle \simeq 0.3\mu_B$. Here, ν_{yx} is the Nernst signal for $\vec{\nabla}T \parallel \hat{x}$. The stripes have a modulation wavevector $\parallel \hat{x}$, i.e. run along $\hat{y}$, such that ν_{xy} (ν_{yx}) is defined with $\vec{\nabla}T$ parallel (perpendicular) to the stripes. (Figure adapted from [25].)

occurs at $t_{1y}/t_{1x} \approx 0.9$, where the electron-like Fermi surface of the isotropic limit changes into open orbits. At the van-Hove singularity, both Nernst signals are enhanced. Interestingly, in the open-orbit regime, ν_{yx}/T remains finite, while ν_{xy}/T tends to zero as $t_{1y} \to 0$. This implies a huge anisotropy of the Nernst signal for open orbits[7]. Recall that ν_{yx} is the Nernst signal for $\vec{\nabla}T \parallel \hat{x}$, that is, a strong Nernst signal occurs for $\vec{\nabla}T$ ($\vec{E}$) parallel (perpendicular) to the strong hopping direction. We note that the same information was already present in figure 3(b) of [27], where a large hopping anisotropy ϵ in an electron-nematic state led to a Lifshitz transition to a Fermi surface with open orbits, resulting in $|\nu_{xy}| \ll |\nu_{yx}|$ as in figure 2.

The limit of small t_{1y} can be understood analytically. Power counting in the Boltzmann expressions for the conductivities shows that $\sigma_{xx}, \alpha_{xx} \propto t_{1y}^0$, while the other quantities $\sigma_{yy}, \sigma_{xy}, \alpha_{yy}, \alpha_{xy}$ scale as t_{1y}^2. From equation (4), it follows that $\nu_{yx} \propto t_{1y}^0$ while $\nu_{xy} \propto t_{1y}^2$, consistent with figure 2. Note that, of course, there is no transverse response for $t_{1y} = 0$, that is, there is no meaningful definition of the Nernst signal in the strict one-dimensional (1D) limit. Finally, the sign of ν_{yx} for small t_{1y} is not robust, but depends on details of the quasi-1D band structure.

5.3. Nernst effect from stripes in underdoped cuprates

Let us start by summarizing the main results obtained previously in [25]. There, mainly stripes with period $M = 8$ and doping levels of 1/8 and higher were considered. For spin stripes with realistic amplitudes of the ordered magnetic moments, $2\mu_B\langle S_z\rangle < 0.3\mu_B$, the Nernst signal was found to be strongly enhanced, with its sign being positive. The result is reproduced in figure 3. Depending on the admixture of charge modulations, sign changes in the Nernst

[7] Hackl *et al* (2010) [25] stated that open orbits do not appreciably contribute to the Nernst signal. While true for some of the stripe states investigated in [25], this is not generally valid; see section 5.2 of the present paper.

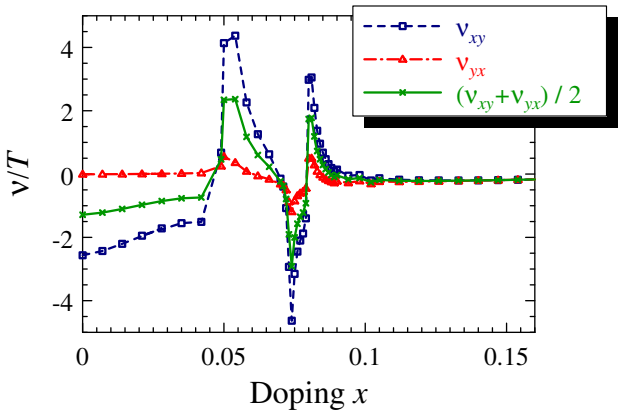

Figure 4. Nernst signal as in figure 3, but now for period-12 antiferromagnetic stripes as a function of doping x. The modulation strength is chosen as $V_s(x) = (0.328 - x)$ eV. The regime of open orbits, $x < 5\%$, is characterized by a strong Nernst anisotropy.

signal occurred as a function of modulation strength or doping. Some calculations were also performed for modulation periods $M = 10$ and 16 appropriate for more underdoped cuprates, with qualitatively similar results, but a robust positive Nernst signal remained restricted to period-8 spin stripes.

For most stripe states investigated in [25], the anisotropy of the Nernst signal was found to be weak. This can be interpreted as arising from the averaging over various anisotropic orbits of the backfolded band structure. This weak anisotropy is in contrast to the huge anisotropy that results from the orthorhombic distortion of a single large Fermi surface sheet in an electron-nematic state [27]. There, a subtle interference of the diagonal anisotropies in the transport tensors $\hat{\sigma}$ and $\hat{\alpha}$ can cause a large Nernst anisotropy even if the anisotropies in σ and α are moderate.

We are now in a position to discuss the Nernst signal from spin stripes for strongly underdoped cuprates as introduced in section 5.1. We again fix $M = 12$, use vertical stripes and employ $V_s(x) = (0.328 - x)$ eV as proposed in [32]. The resulting Nernst coefficients ν/T for both directions are displayed in figure 4. Most strikingly, the signal is strongly enhanced at the various Lifshitz transitions at $x \approx 5$, 7.5 and 8.5%; see section 5.1. (Note that jumps in ν/T occur at Lifshitz transitions where Fermi pockets open or close; this has been analyzed in some detail in [24].)

At dopings $x > 10\%$, the extended pockets lead to a small Nernst signal with little anisotropy. In the opposite limit of small dopings $x < 5\%$, only ν_{xy} is sizeable while ν_{yx} is tiny—this is consistent with the discussion in section 5.2, with the difference that here the open Fermi orbits run in the $\hat{x}$ direction, while they run along $\hat{y}$ for small t_{1y} in section 5.2. The emergence of hole pockets at $x \approx 5\%$ then leads to a large positive Nernst signal, which changes sign multiple times upon further increasing x where electron pockets emerge, figure 1. All features are much more pronounced in ν_{xy} compared to ν_{yx}, reflecting in general the quasi-1D character of Fermi surfaces.

6. Discussion

In this paper, we have summarized [25, 27] and extended the analysis of the Nernst signal from quasiparticles in cuprates with broken lattice symmetries. For stripe states, we find the quasiparticle Nernst signal ν/T to be significantly enhanced (compared to the unmodulated state), which can be traced back to the presence of small Fermi pockets. The sign of ν/T depends on the period and strength of the modulation and other microscopic details, with a positive ν/T being found for period-8 spin stripes. In the small-doping regime, where the Fermi surface of the stripe state consists of open orbits only, the Nernst signal in one direction is tiny, while in the other it is strongly negative. The latter is in fact the only case where a robust and large anisotropy in the stripe-induced Nernst signal was found. Note that for nematic distortion of a single Fermi surface sheet, Nernst anisotropy is robustly large, in particular near a van-Hove singularity [27].

6.1. Robustness

As our calculations involved a series of approximations, one may ask which features can be expected to be robust. The two most drastic approximations are probably (i) the mean-field approximation for the ordered states and (ii) the relaxation-time approximation with constant τ_0.

At present, it is difficult to estimate the effects of order-parameter fluctuations beyond mean field (i). However, a better understanding of those might be needed in particular in the context of fluctuating stripes, which have been suggested to occur at elevated temperatures in various cuprates. In contrast, deep in the ordered state, we can assume the mean-field approximation to be qualitatively justified.

Approximation (ii) neglects both the temperature and energy dependence and the anisotropy of the relaxation rate. The angular dependence of τ_0 may well be important for the Nernst response of stripe states, because all conductivities receive contributions from the various Fermi pockets, which will in general have different relaxation rates. Hence, the enhancement of the Nernst signal near van-Hove singularities and Lifshitz transitions can be expected to be robust, but the sign of the Nernst signal away from these singularities may change upon including anisotropic scattering. Importantly, our qualitative conclusions for Nernst anisotropies are rather robust: for instance, for the electron-nematic order discussed in [27], only a strong difference in scattering rates at $(\pi, 0)$ and $(0, \pi)$ could spoil the result, which is unlikely.

6.2. Experiments

Nernst effect investigations in 214 cuprates have an extended history, and the enhanced positive Nernst signal at intermediate temperatures above T_c has been commonly interpreted as a signature of vortex physics, i.e. preformed Cooper pairs [15, 16]. The recent identification [17] of an additional positive contribution, whose temperature dependence appears to track some characteristic pseudogap (or charge order) scale, has been qualitatively verified by others [64], but its interpretation [17] in terms of a Fermi-surface reconstruction due to charge order has been questioned [18, 64].

Our results, showing a positive Nernst signal for period-8 stripes [25], are in principle consistent with this interpretation. However, the fact that only minor differences in the Nernst

signal exist between stripe-ordered $La_{1.8-x}Eu_{0.2}Sr_xCuO_4$ and $La_{1.6-x}Nd_{0.4}Sr_xCuO_4$ on the one hand and non-stripe-ordered $La_{2-x}Sr_xCuO_4$ on the other hand [17, 64] complicates matters. As $La_{2-x}Sr_xCuO_4$ is expected to have strong stripe *fluctuations*, a scenario of fluctuating stripes [5, 65] being responsible for Nernst enhancement is viable, but a concrete theoretical analysis (which also has to account for pinning of stripes by defects) is lacking.

For underdoped YBCO, the Nernst signal is negative and strongly anisotropic in a doping-dependent window of intermediate temperatures [20]. This appears to be consistent with the results of [27], supporting the interpretation that electron-nematic order is at play in YBCO (with the built-in orthorhombicity acting as a field that smears the nematic phase transition and aligns the domains).

Nernst measurements on more underdoped YBCO should be extremely interesting, in particular in a regime where field-induced incommensurate magnetism has been detected [57] and where the superconducting T_c is small. Then, one can expect that our results for long-period spin stripes become relevant. Based on figure 4, we predict that at low doping also the low-temperature Nernst signal should be strongly anisotropic, with ν_{yx} (ν_a in the terminology of [20]) being tiny (assuming that the stripes run along the orthorhombic b axis [7, 21]).

Acknowledgments

We acknowledge useful discussions as well as collaborations on related subjects with L Fritz, A Rosch, S Sachdev, L Taillefer and A Wollny. This research was supported by the DFG through SFB 608 (Köln) and the Research Units FOR 538 and FOR 960.

References

[1] Timusk T and Statt B W 1999 *Rep. Prog. Phys.* **62** 61
[2] Norman M R, Pines D and Kallin C 2005 *Adv. Phys.* **54** 715
[3] Lee P A, Nagaosa N and Wen X-G 2006 *Rev. Mod. Phys.* **78** 17
[4] Emery V J, Kivelson S A and Tranquada J M 1999 *Proc. Natl Acad. Sci. USA* **96** 8814
[5] Kivelson S A, Bindloss I P, Fradkin E, Oganesyan V, Tranquada J M, Kapitulnik A and Howald C 2003 *Rev. Mod. Phys.* **75** 1201
[6] Castro Neto A H and Morais Smith C 2004 *Strong Interactions in Low Dimensions* ed D Baeriswyl and L Degiorgi (Dordrecht: Kluwer) p 277
[7] Vojta M 2009 *Adv. Phys.* **58** 699
[8] Tranquada J M, Sternlieb B J, Axe J D, Nakamura Y and Uchida S 1995 *Nature* **375** 561
[9] Howald C, Eisaki H, Kaneko N, Greven M and Kapitulnik A 2003 *Phys. Rev.* B **67** 014533
[10] Vershinin M, Misra S, Ono S, Abe Y, Ando Y and Yazdani A 2004 *Science* **303** 1995
[11] Kohsaka Y *et al* 2007 *Science* **315** 1380
[12] Caroli C and Maki K 1967 *Phys. Rev.* **164** 591
Maki K 1968 *Phys. Rev. Lett.* **21** 1755
[13] Mukerjee S and Huse D A 2004 *Phys. Rev.* B **70** 014506
[14] Behnia K *J. Phys.: Condens. Matter* **21** 113101
[15] Xu Z A, Ong N P, Wang Y, Kakeshita T and Uchida S 2000 *Nature* **406** 486
[16] Wang Y, Li L and Ong N P 2006 *Phys. Rev.* B **73** 024510
[17] Cyr-Choinière O *et al* 2009 *Nature* **458** 743
[18] Li L, Wang Y, Komiya S, Ono S, Ando Y, Gu G D and Ong N P 2010 *Phys. Rev.* B **81** 054510
[19] Chang J *et al* 2010 *Phys. Rev. Lett.* **104** 057005

[20] Daou R *et al* 2010 *Nature* **463** 519
[21] Hinkov V, Haug D, Fauqué B, Bourges P, Sidis Y, Ivanov A, Bernhard C, Lin C T and Keimer B 2008 *Science* **319** 597
[22] Oganesyan V and Ussishkin I 2004 *Phys. Rev.* B **70** 054503
[23] Tewari S and Zhang C 2009 *Phys. Rev. Lett.* **103** 077001
[24] Hackl A and Sachdev S 2009 *Phys. Rev.* B **79** 235124
[25] Hackl A, Vojta M and Sachdev S 2010 *Phys. Rev.* B **81** 045102
[26] Zhang C, Tewari S and Chakravarty S 2010 *Phys. Rev.* B **81** 104517
[27] Hackl A and Vojta M 2009 *Phys. Rev.* B **80** 220514
[28] Millis A J and Norman M R 2007 *Phys. Rev.* B **76** 220503
[29] Dimov I, Goswami P, Jia X and Chakravarty S 2008 *Phys. Rev.* B **78** 134529
[30] Lin J and Millis A J 2008 *Phys. Rev.* B **78** 115108
Lin J and Millis A J 2009 *Phys. Rev.* B **80** 193107
[31] Harrison N 2009 *Phys. Rev. Lett.* **102** 206405
[32] Norman M R, Lin J and Millis A J 2010 *Phys. Rev.* B **81** 180513
[33] Sebastian S E, Harrison N, Altarawneh M M, Mielke C H, Liang R, Bonn D A, Hardy W N and Lonzarich G G 2010 *Proc. Natl Acad. Sci. USA.* **107** 6175
[34] Christensen N B, Rønnow H M, Mesot J, Ewings R A, Momono N, Oda M, Ido M, Enderle M, McMorrow D F and Boothroyd A T 2007 *Phys. Rev. Lett.* **98** 197003
[35] Kivelson S A, Fradkin E and Emery V J 1998 *Nature* **393** 550
[36] Emery V J and Kivelson S A 1993 *Physica* C **209** 597
[37] Kivelson S A and Emery V J 1993 *Strongly Correlated Electronic Materials: The Los Alamos Symp.* ed K S Bedell, Z Wang, D E Meltzer, A V Balatsky and E Abrahams (Reading, MA: Addison-Wesley) p 619
[38] Castellani C, Di Castro C and Grilli M 1995 *Phys. Rev. Lett.* **75** 4650
[39] Zaanen J, Horbach M L and van Saarloos W 1996 *Phys. Rev.* B **53** 8671
[40] Sachdev S 2003 *Rev. Mod. Phys.* **75** 913
[41] Vojta M and Sachdev S 1999 *Phys. Rev. Lett.* **83** 3916
[42] Sebastian S E, Harrison N, Altarawneh M M, Liang R, Bonn D A, Hardy W N and Lonzarich G G 2010 *Phys. Rev.* B **81** 140505
[43] Ramshaw B J, Vignolle B, Day J, Liang R, Hardy W N, Proust C and Bonn D A 2010 arXiv:1004.0260
[44] Senthil T, Sachdev S and Vojta M 2003 *Phys. Rev. Lett.* **69** 216403
[45] Haule K and Kotliar G 2007 *Phys. Rev.* B **76** 092503
[46] Vidhyadhiraja N S, Macridin A, Sen C, Jarrell M and Ma M 2009 *Phys. Rev. Lett.* **102** 206407
[47] Civelli M, Capone M, Georges A, Haule K, Parcollet O, Stanescu T D and Kotliar G 2008 *Phys. Rev. Lett.* **100** 046402
[48] Sakai S, Motome Y and Imada M 2009 *Phys. Rev. Lett.* **102** 056404
[49] Yang K-Y, Rice T M and Zhang F-C 2006 *Phys. Rev.* B **73** 174501
[50] Fournier D *et al* 2010 arXiv:1007.4027
[51] Sondheimer E H 1948 *Proc. R. Soc.* A **193** 484
[52] Varma C M, Yakovenko V M and Kapitulnik A 2010 arXiv:1007.1215
[53] Norman M R, Randeria M, Ding H and Campuzano J C 1994 *Phys. Rev.* B **52** 615
[54] Andersen O K, Liechtenstein A I, Jepsen O and Paulsen F 1995 *J. Phys. Chem. Solids* **56** 1573
[55] Vojta M and Rösch O 2008 *Phys. Rev.* B **77** 094504
[56] Chang J *et al Phys. Rev. Lett.* **102** 177006
[57] Haug D *et al* 2009 *Phys. Rev. Lett.* **103** 017001
[58] Demler E, Sachdev S and Zhang Y 2001 *Phys. Rev. Lett.* **87** 067202
[59] LeBoeuf D *et al* 2007 *Nature* **450** 533
[60] Doiron-Leyraud N, Proust C, LeBoeuf D, Levallois J, Bonnemaison J-B, Liang R, Bonn D A, Hardy W N and Taillefer L 2007 *Nature* **447** 565

[61] Sebastian S E, Harrison N, Palm E, Murphy T P, Mielke C H, Liang R, Bonn D A, Hardy W N and Lonzarich G G 2008 *Nature* **454** 200
[62] Audouard A, Jaudet C, Vignolles D, Liang R, Bonn D A, Hardy W N, Taillefer L and Proust C 2009 *Phys. Rev. Lett.* **103** 157003
[63] Yamada K *et al* 1998 *Phys. Rev.* B **57** 6165
[64] Hess C, Ahmed E M, Ammerahl U, Revcolevschi A and Büchner B 2010 arXiv:1006.2846
[65] Vojta M, Vojta T and Kaul R K 2006 *Phys. Rev. Lett.* **97** 097001